Journal of Materials Chemistry A

Thermoelectric properties and low thermal conductivity of Zintl compound $Yb_{10}MnSb_9$

Journal:	*Journal of Materials Chemistry A*
Manuscript ID	TA-ART-04-2022-003114.R1
Article Type:	Paper
Date Submitted by the Author:	23-Jun-2022
Complete List of Authors:	Borgsmiller, Leah; Northwestern University, Materials Science and Engineering Snyder, G.; Northwestern University, Materials Science

Journal Name

ARTICLE TYPE

Cite this: DOI: 00.0000/xxxxxxxxxx

Thermoelectric Properties and Low Thermal Conductivity of Zintl Compound $Yb_{10}MnSb_9$

Leah Borgsmiller,[a] and G. Jeffrey Snyder,*[a]

Received Date
Accepted Date

DOI: 00.0000/xxxxxxxxxx

The recently discovered Zintl compound $Yb_{10}MnSb_9$ is a thermoelectric material very close in compositional space to high performing thermoelectric materials such as $Yb_{14}MnSb_{11}$ and $Yb_{21}Mn_4Sb_{18}$. Here we measure and report electronic and thermal transport data for $Yb_{10}MnSb_9$ up to 825K. Due to the complicated crystal structure, this material has ultralow thermal conductivity. The ultralow lattice thermal conductivity in conjunction with a higher Seebeck coefficient than in other Yb-Mn-Sb compounds, leads to a moderate zT of about 0.34 at 825K and is likely to peak at a higher value via material optimization. We approximate a bandgap of about 0.4 eV and expect the zT to be able to reach values as high as 0.33 at 725K (which is comparable to $Yb_{14}MnSb_{11}$ at that temperature) using a thermoelectric quality factor analysis. This zT has the potential to reach even higher values by improving the quality factor, B, through grain boundary engineering. Here we provide suggestions for future studies to improve thermoelectric performance. This work is the first report of thermal conductivity, bandgap, and zT for this $Yb_{10}MnSb_9$ compound, and we discuss implications of this material for future thermoelectric study through comparisons to the leading $Yb_{14}MnSb_{11}$ material.

1 Introduction

Thermoelectrics are materials that take a temperature gradient and convert it to electricity and vice versa. Thermoelectric materials that operate at high temperatures are essential for applications such as powering deep space vehicles[1]. However, the improvement of thermoelectric performance, measured by the dimensionless figure of merit zT ($zT = \frac{\alpha^2 T}{\sigma\kappa}$), requires optimization of often conflicting material properties (electrical conductivity (σ), Seebeck coefficient (α), and thermal conductivity (κ))[2].

Zintl compounds are a specific type of material first considered by Eduard Zintl[3–5]that include many thermoelectric materials such as 14-1-11 compounds[6–9], Ca_3AlSb_3[10], $Ba_8Ga_{16-x}Ge_{30+x}$ clathrates[11], Mg_3Sb_2[12], Mg_2Si[13], ZnSb[14], Zn_4Sb_3[15,16], and filled skutterudites[17]. These materials exist along the border between metallic and nonmetallic behavior and have unit cells consisting of electronegative anions with electropositive cations that donate their valence electrons[18,19]. Some earlier definitions require polyanionic frameworks[18], while others consider a broader definition allowing materials like Mg_3Sb_2 to be considered Zintl. Zintl compounds follow simple valence counting rules[20]. Many different Zintl compounds have complicated unit cells resulting in intrinsically low lattice thermal conductivity[21]. This along with their interesting electronic properties, makes many Zintl compounds desirable as thermoelectric materials[16,22].

The Zintl compound $Yb_{14}MnSb_{11}$[23], has been the topic of numerous studies[6,8,9,24–26] due to its high thermoelectric performance at high temperatures making it a desirable candidate for space applications. This compound exists in the complicated Yb-Mn-Sb phase diagram which includes many binary and ternary compounds, with multiple Zintl compounds displaying thermoelectricity. This Yb-Mn-Sb phase diagram is shown in Figure 1. $Yb_{14}MnSb_{11}$, $Yb_{21}Mn_4Sb_{18}$[27], and the newly discovered[28] $Yb_{10}MnSb_9$ phases are all p-type Zintl thermoelectric materials very close to each other in compositional space.

$Yb_{10}MnSb_9$ was recently discovered and has been shown in an introductory study to have a Seebeck coefficient higher than that of other phases in the Yb-Mn-Sb system[28]. It was hypothesized to have a low lattice thermal conductivity, κ_L, due to its complicated unit cell. The crystal structure as determined by Baranets et al. is tetragonal in the $P4_2/mnm$ space group and is related to the $Ca_{10}LiMgSb_9$ crystal structure but with additional structural disorder[28]. Other materials in this crystal structure are $Ca_{10}MSb_9$ (M= Ga, In, Mn, Zn)[29], and $A_2Ca_{10}Sb_9$ (A = Li, Mg)[30]. While the phase is discussed using the stoichiometry $Yb_{10}MnSb_9$, the actual composition may be more complex as previous single crystal XRD analysis has suggested that the stoichiometry is $Yb_{10.90}Mn_{0.48}Sb_9$[28], resulting from partial occupancies on some of the Yb and Mn sites. Note that this crystal structure is different from the orthorhombic *Iba2* spacegroup structure observed in other Zintl antimonides including $Yb_{11}GaSb_9$[31,32], $Yb_{11}InSb_9$[32,33], $Yb_{11}AlSb_9$[34], and $Eu_{11}InSb_9$[33]. In this work, we

[a] Northwestern University, Department of Materials Science and Engineering, Evanston, IL 60208
* Email: jeff.snyder@northwestern.edu

confirm the hypothesized low thermal conductivity and report higher temperature transport data in order to consider the potential of this material as a high temperature thermoelectric and consider how this relates to $Yb_{14}MnSb_{11}$ and future optimization studies.

2 Methods

2.1 Synthesis

Polycrystalline pellets were synthesized through a high energy ball-milling and hot pressing synthesis route. To start, elemental Mn was purified by annealing in a sealed quartz ampule with quartz wool at 1000 °C for 12 hours, in order to remove oxide from the Mn pieces. Then, a MnSb precursor compound was synthesized by combining equal mole ratios of purified Mn and Sb shot (99.999%, 5N Plus) and then annealing in a quartz tube by ramping to 950°C at a rate of 100°C/min followed by a two hour dwell before bringing the temperature down to 675°C and holding the temperature there for 48 hours before quenching. The Mn and Sb were confirmed to have fully reacted forming MnSb using powder x-ray diffraction (XRD). This precursor step was conducted to better allow for a complete reaction and to minimize the presence of secondary phases in the final product. The use of MnSb as a precursor material has been used in multiple $Yb_{14}MnSb_{11}$ studies[6,41] to allow for phase pure synthesis and the use of multiple binaries in synthesizing 14-1-11 compounds has been thoroughly investigated as a means of encouraging complete chemical reactions[42]. Yb shavings were obtained by using a steel rasp to file a large Yb ingot in an Ar glovebox. Then, the synthesized MnSb, Sb shot and Yb shavings were combined in the molar ratio Yb:Mn:Sb = 10.5:1.125:9 for a total of 6.5 grams.

The powder was then ballmilled in a stainless steel jar sealed in an Argon glovebox with an O-ring in a SPEX high energy ball mill for a total of 270 minutes, with the ball mill jar taken out every 90 minutes to scrape the powder off the sides of the wall using steel spatulas and tools.

In order to make a dense polycrystalline pellet, the powder was then loaded into a half inch diameter graphite die and was pressed in a rapid RF induction heating hot press instrument[43] for 30 min at 45 MPa and 900°C. A single pressed pellet contained approximately 2.3 grams of powder. The pellets were then polished using polishing papers of various grit sizes. The density was measured using isopropyl alcohol and the Archimedes method and was determined to be 8.21 g/cm^3.

2.2 X-Ray Diffraction (XRD) Measurements

X-Ray Diffraction (XRD) measurements on bulk polycrystalline samples were conducted using a Stoe STADI-MP instrument. Pure Cu Kα1 radiation was used in reflection mode. A scan in 2θ from 20° to 84° was conducted with a scan time of about 20 minutes in total.

2.3 Transport Measurements

The electrical resistivity and conductivity was measured up to 825K using a home-built Hall instrument using the Van der Pauw method with details of the instrument set-up described elsewhere[44]. Similarly, the Seebeck coefficient was measured using Chromel-Nb thermocouples up to 825K using a home-built instrument described in Iwanaga et al[45].

The thermal diffusivity was measured using a commercial laser flash analysis (LFA) instrument (Netzsch LFA 457 *MicroFlash*.) The thermal conductivity was then calculated from the thermal diffusivity using the measured density and the Dulong-Petit approximation for heat capacity.

3 Results and Discussion

After synthesizing polycrystalline pellets, the crystal structure was confirmed using XRD. The X-ray diffraction patterns for both the experimental diffraction peaks and the calculated diffraction pattern using crystallographic information from Baranets et al.[28] and a basic Rietveld refinement[46] are shown in Figure 2 and show overall good agreement. Rietveld refinement steps were taken using the GSAS-II software[47]. Here we received a final R_w value of 13%. The refined lattice parameters were a=11.80443 Å and c=17.11809 Å , which is very similar to those reported previously[28] (a=11.8336(17) Å and c=17.043(3) Å). Slight discrepancies in these lattice parameters could be due to slightly different atomic site occupancies or due to thermal differences.

It should be noted that the stoichiometry used in synthesis was not the same as suggested by the single crystal XRD analysis by Baranets et al.[28]. When samples were made using the refined stoichiometry of Yb:Mb:Sb=10.9:0.48:9, the x-ray diffraction patterns did not match the expected crystal structure and many secondary phases were present (see Figure S1 in the supplemental information). Thus, here our reported data corresponds to a sample made by synthesis with the following ratio of the elements, Yb:Mn:Sb = 10.5:1.125:9. This is close to the experimental nominal composition from Baranets et al.[28] of Yb:Mn:Sb= 10.75:0.75:9 with slightly more Mn. This excess Mn used in synthesis may be necessary for reaction, as it may be easy to systematically lose Mn during synthesis. This may be similar to the case of $Yb_{14}MnSb_{11}$ where a slight excess of Mn is frequently used as it improves thermoelectric performance[6]. Additionally there may be more Mn in the composition of this phase than what was previously reported which could be contributing to these slightly differing lattice parameters. Thus far, the role of the excess Mn in synthesizing $Yb_{10}MnSb_9$ has not been completely uncovered, yet it is apparent that both this and the previous report required some excess Mn in synthesis of bulk samples in comparison to the stoichiometry determined via single crystal XRD.

Measurements of both the electronic and thermal properties of $Yb_{10}MnSb_9$ from room temperature up to about 825K are reported here in Figures3 and 4.

The key strength of $Yb_{10}MnSb_9$ as a thermoelectric material is the thermal properties which are shown in Figure 3. Figure 3a depicts the total thermal conductivity as determined from LFA diffusivity measurements, whereas Figure 3b, shows the lattice thermal conductivity which was determined by subtracting the electronic contribution to the total thermal conductivity determined using the electrical resistivity and the Lorenz number.

Here it is observed that $Yb_{10}MnSb_9$ has an ultralow thermal conductivity, even lower than that of $Yb_{14}MnSb_{11}$, which has one

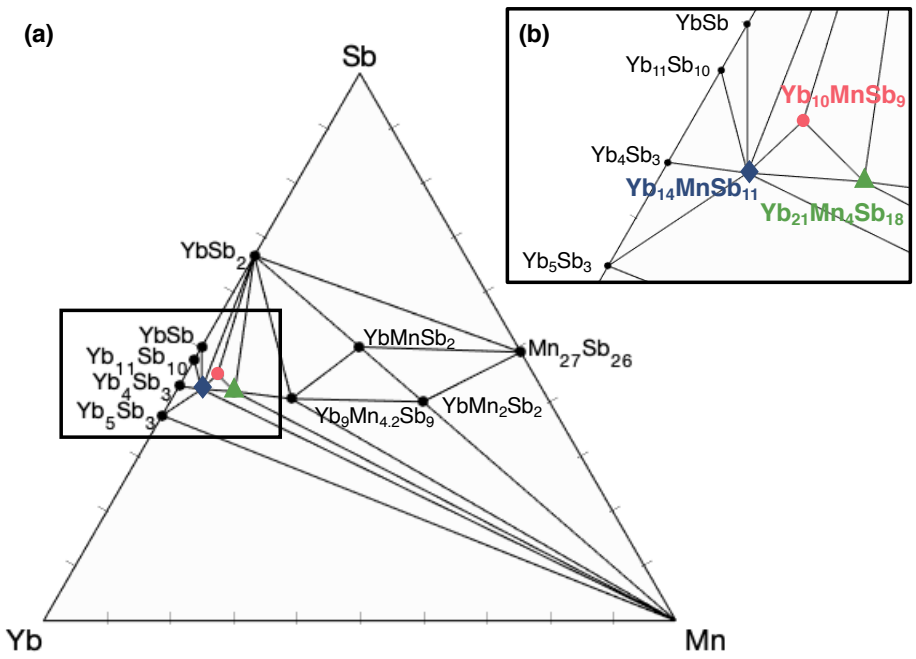

Fig. 1 (a) Ternary phase diagram for the Yb-Mn-Sb system. The inset (b) shows a zoomed in portion of the phase diagram consisting of the thermoelectric Zintl phases $Yb_{14}MnSb_{11}$[23], $Yb_{21}Mn_4Sb_{18}$[27], and $Yb_{10}MnSb_9$[28]. Other reported ternary phases in this system are $Yb_9Mn_{4.2}Sb_9$[35], $YbMnSb_2$[36], and $YbMn_2Sb_2$[37]. Stable binary phases have been reported by Materials Project[38] and the Open Quantum Materials Database (OQMD)[39,40].

of the lowest thermal conductivities of practical thermoelectric materials. However, when considering the only the lattice contributions to the total thermal conductivity, the lattice thermal conductivity of $Yb_{14}MnSb_{11}$ is lower than that of $Yb_{10}MnSb_9$, although the κ of $Yb_{14}MnSb_{11}$ appears to be affected by multiple electronic bands making it less clear how to extract a lattice contribution[26]. The total thermal conductivity of $Yb_{10}MnSb_9$ appears to be completely dominated by the lattice thermal conductivity term and thus the values for total thermal conductivity and lattice thermal conductivity are nearly identical. This is because this material has a very high electrical resistivity, and as such very little heat is carried by the electronic charge carriers. The low lattice thermal conductivity is attributed to the complicated crystal structure with partial occupancies. The complex, disordered structure is expected to have thermal conductivity dominated by diffuson as opposed to propagating phonon which give a nearly temperature independent κ as observed even in crystalline $Yb_{14}MnSb_{11}$[48].

The measured electronic transport data in the form of the electrical resistivity and Seebeck coefficient are shown here in Figure 4. We compare the data here with data both previously reported for this material[28], as well as data from the well-studied high temperature thermoelectric $Yb_{14}MnSb_{11}$[24]. In general, $Yb_{10}MnSb_9$ has both a higher Seebeck coefficient and a higher electrical resistivity than $Yb_{14}MnSb_{11}$. The Seebeck coefficient for $Yb_{10}MnSb_9$ demonstrates the onset of bipolar conduction around 750K which is shown by the turnover in the Seebeck. Additionally, it should be noted that while the $Yb_{10}MnSb_9$ sample reported here follows the same general trend with temperature as that reported previously[28], it demonstrated both a higher electrical resistivity and a higher Seebeck coefficient. This can likely be attributed to these samples having a different charge carrier concentration. That is, there is likely a lower concentration of charge carriers in the sample reported here than the sample reported previously. Additionally, the difference in charge carrier concentration between the sample measured here and the work of Baranets et al.[28] (as suggested by the higher electrical conductivity and Seebeck coefficient values exhibited by our sample) suggests that the addition of excess Mn may be changing the phase equilibria, thus impacting charge carrier concentration.

This phase equilibria dependent carrier concentration has been found in numerous phase boundary mapping studies[49]. In short, by changing the phase equilibria, the chemical potentials of thermoelectric samples can be set, which can have profound impacts on defect energies and thus charge carrier concentrations[50–55]. For instance, it has been shown that in the Zintl compound $Ca_9Zn_{4+x}Sb_9$, the carrier concentration can be changed by more than an order of magnitude just through very small changes in the Zn content[50]. Future work on this compound could utilize a complete phase boundary mapping approach to optimize this material. This would involve purposefully synthesizing samples off-stoichiometry to sample the thermoelectric properties that are present for samples synthesized in different three phase regions on the ternary phase diagram.

The electronic band structure of this material has not yet been

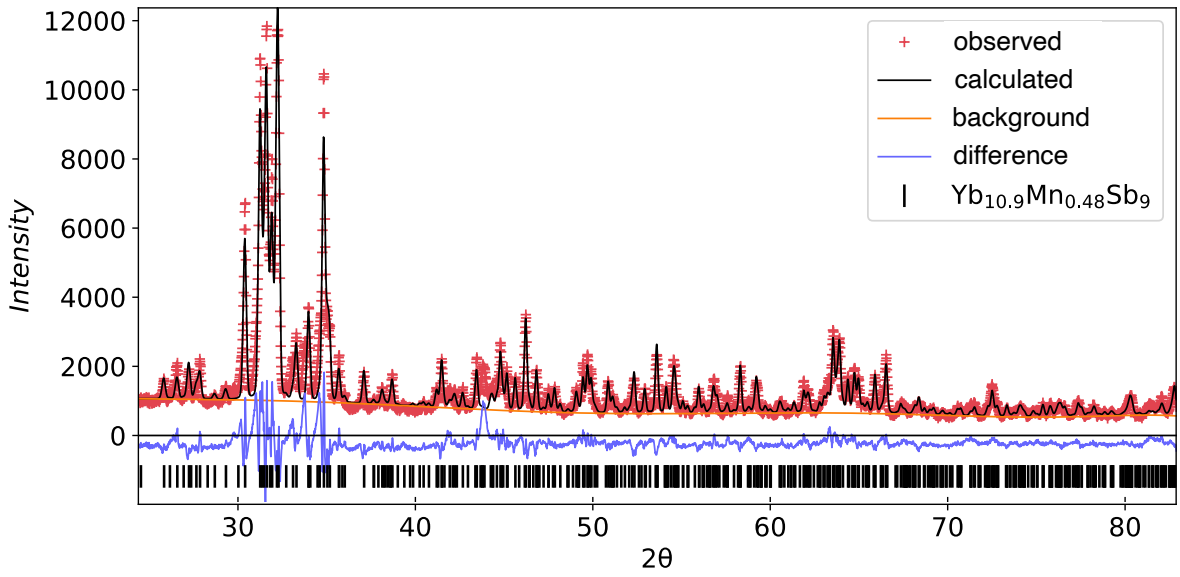

Fig. 2 Observed X-ray diffraction pattern found using a Stadi-MP with Cu radiation in reflection mode on a bulk sample. Here the red points correspond to observed data, the black curve corresponds to the calculated diffraction pattern found using the crystallographic information file from Baranets et al.[28] as well as a Rietveld refinement fit. The blue line is the difference between the observed and calculated curve, which shows fairly good agreement throughout and minimal secondary phases (although there does appear to be an unidentifiable extra peak around 43.75°). The black vertical lines indicate all of the angles with expected peaks from the crystal structure.

reported, however the bandgap can be approximated from the peak in the Seebeck coefficient and the corresponding temperature using the Goldsmid-Sharp approximation[56].

$$E_g \approx 2e|S_{max}|T_{max} \tag{1}$$

Using the peak in Seebeck determined experimentally (Figure 4), this bandgap was approximated to be about 0.4 eV. This bandgap value is comparable to bandgaps of other thermoelectric materials in this Yb-Mn-Sb system, such as $Yb_9Mn_{4.2}Sb_9$ (0.4 eV)[57], $Yb_{14}MnSb_{11}$ (0.5 eV)[24], and $Yb_{21}Mn_4Sb_{18}$ (0.4 eV)[27].

The thermoelectric quality factor, B, is a way to consider the maximum zT a material can achieve given appropriate doping. This quality factor is useful in comparing unoptimized materials and is proportional to the weighted mobility divided by the lattice thermal conductivity ($B \sim \mu_w/\kappa_L$)[58,59]. The weighted mobility can be calculated from Seebeck coefficient and electrical conductivity measurements[58]. If we consider the temperature where the weighted mobility peaks before the onset of bipolar conduction (725K as shown in Figure 5a), we can calculate the corresponding thermoelectric quality factor B to approximate the theoretical maximum zT for that temperature[60]. A B value of about 0.10 was calculated for the experimental $Yb_{10}MnSb_9$ at 723K using the following equation, where k_B is the Boltzmann constant, κ_L is the lattice thermal conductivity, T is the temperature, and σ_{Eo} is the transport coefficient[60].

$$B = (\frac{k_B}{e})^2 \frac{\sigma_{Eo}}{\kappa_L} T \tag{2}$$

The transport coefficient can be calculated for a material at a given temperature using measurements of the Seebeck coefficient and the electrical conductivity with the following analytic equation which is accurate within 5% when the absolute value of the Seebeck coefficient is greater than 120μV/K[60].

$$\sigma_{Eo} = \sigma \cdot exp[\frac{|S|}{k_B/e} - 2] \tag{3}$$

Using this calculated B value, the relationship between zT and the reduced chemical potential, $\eta = E_F/k_BT$ can be determined using the following equation[60] which is plotted in Figure 5b.

$$zT = \frac{S^2(\eta)}{\frac{(k_B/e)^2}{Bln(1+e^{\eta})} + L(\eta)} \tag{4}$$

From this it can be determined that given optimized doping, $Yb_{10}MnSb_9$ should be able to reach a zT of 0.33 at 725K. This is approaching the zT of $Yb_{14}MnSb_{11}$ at this temperature which as measured by Brown et al.[24] is about 0.36.

Thus, further doping may be necessary to optimize the charge carrier concentration and overall performance. The Seebeck coefficient for this material is quite high, indicating that this sample is underdoped and that future optimization would require a decrease in the charge carrier concentration. This stands in contrast to $Yb_{14}MnSb_{11}$ where the pure compound has too high of a carrier concentration and optimization efforts generally involve attempts to decrease the carrier concentration[8,41,61,62] (although this approach may have been flawed as recent studies on the multi-band

effect in 14-1-11 compounds suggests that a reduction in n may not be necessary[26]). While this material has been shown to have multiple sites with partial occupancies[28], with the right dopants attempts could still be made to decrease the carrier concentration sufficiently to reach optimal performance. Doping on the Yb site would likely be the best option because there are fractionally less Yb sites with partial occupancies. Doping this site with a $+1$ cation such as Na^{+1} could allow for the tuning of the carrier concentration.

In Figure 5, it can also be seen that the weighted mobility for this material is quite low compared to high performing materials in this system. One way that this could be improved is through a reduction of spin-disorder scattering through partial substitution of Zn on the Mn site. Since Mn and Zn cations are isoelectronic, while Mn has magnetic properties and Zn does not, substituting some of the Mn atoms with Zn can allow for a reduction in spin disorder scattering without changing the carrier concentration or other electronic properties very much. This has been a successful route in improving thermoelectric performance in $Yb_{14}MnSb_{11}$[63] and has been shown to improve carrier mobility in $Yb_9Mn_{4.2}Sb_9$[64] and thus would be a good starting point to potentially improve the weighted mobility of this material.

The zT of the experimental $Yb_{10}MnSb_9$ reported here is compared to that of reported $Yb_{14}MnSb_{11}$[24] is shown in Figure 6. The zT at 825K is about 0.34, and it may peak at an even high temperature, similar to $Yb_{14}MnSb_{11}$. Due to the possibly lower bandgap an earlier onset of bipolar conduction in $Yb_{10}MnSb_9$ suggests that the zT will not peak at as high of a temperature as $Yb_{14}MnSb_{11}$ given its current level of doping. However, when optimally doped, $Yb_{10}MnSb_9$ will likely exhibit a turnover in the Seebeck coefficient at a higher temperature, closer to that which is seen in the 14-1-11 compound. While the zT of $Yb_{14}MnSb_{11}$ is higher than the ones reported here for $Yb_{10}MnSb_9$, this material has not yet been optimized in any way so there is potential for further increases in zT with a deeper materials study. We have shown that in the mid-temperature range ($\sim$725K), $Yb_{10}MnSb_9$ has the potential given appropriate doping to reach zT values close to that of experimental values for $Yb_{14}MnSb_{11}$. Additionally, our transport data for this material has a very high thermally activated electrical resistivity while having a Seebeck coefficient trend that appears metallic at low temperatures. This suggests substantial grain boundary resistance in these samples[65]. This means that the quality factor for $Yb_{10}MnSb_9$ has the potential to reach even higher values of B thus increasing the maximum zT through grain growth[65,66] or other grain boundary engineering techniques[67–69]. This suggests that the optimized zT of $Yb_{10}MnSb_9$ has the potential to surpass $Yb_{14}MnSb_{11}$, making it one of the best materials in this temperature range.

Additionally, $Yb_{10}MnSb_9$ is an important material for us to study and be aware of, particularly in future studies of $Yb_{14}MnSb_{11}$. In Baranets et al.[28], they show that the XRD pattern for $Yb_{10}MnSb_9$ is incredibly similar to $Yb_{11}Sb_{10}$, and thus it is likely that researchers have misidentified secondary phases of $Yb_{10}MnSb_9$ as $Yb_{11}Sb_{10}$. Because $Yb_{10}MnSb_9$ is so close in compositional space to $Yb_{14}MnSb_{11}$, it is likely that secondary phases of $Yb_{10}MnSb_9$ may be present in $Yb_{14}MnSb_{11}$ samples, depending on synthesis route. A greater understanding and awareness of this phase will be essential in future improvements of $Yb_{14}MnSb_{11}$ performance.

To date, this $Yb_{10}MnSb_9$ phase is the only reported compound with the 10-1-9 crystal structure containing Yb. However, we have found evidence for other existing compounds in this family, namely $Yb_{10}MgSb_9$. In previous work studying interstitial Na as a donor in $Yb_{14}MgSb_{11}$, there was an unexplained crystal structure that formed upon doping with Na[70]. The XRD pattern did not match closely with the target 14-1-11 phase, and thus it was concluded that the Na lead to the synthesis of a different compound. In comparing this unidentifiable XRD crystal structure pattern to that of $Yb_{10}MnSb_9$, a high degree of agreement was observed. This suggests that there is likely an Mg analog to this 10-1-9 structure that could be further explored.

4 Conclusions

In this work we synthesized $Yb_{10}MnSb_9$ and measured and reported the thermal and electronic transport properties up to 825K. This material has an ultralow lattice thermal conductivity as a result of the complicated unit cell with partial occupancy sites, with a total thermal conductivity even lower than that of $Yb_{14}MnSb_{11}$. Additionally, in consideration of the thermoelectric quality factor, B, given the quality factor, B, reported here it is unlikely that the thermoelectric figure of merit zT of $Yb_{10}MnSb_9$ will surpass that of $Yb_{14}MnSb_{11}$ with doping alone due to the low weighted mobility, μ_w. However, there is evidence for some grain boundary resistance, and such further material improvements could be made through grain boundary engineering and doping, giving $Yb_{10}MnSb_9$ the potential to surpass the zT of $Yb_{14}MnSb_{11}$ This material is also important to consider when studying properties of other Yb-Mn-Sb thermoelectrics and is likely to appear as a second phase during some synthesis routes of $Yb_{14}MnSb_{11}$. Additionally we suggest that there may be other unreported materials in this structure family, particularly $Yb_{10}MgSb_9$.

Author Contributions

LB conducted all experimental work. Both authors contributed to discussions and the manuscript. GJS supervised the work.

Conflicts of interest

There are no conflicts to declare.

Acknowledgements

LB was supported by the National Science Foundation Graduate Research Fellowship Program under Grant No. DGE-1842165. Any opinions, findings, and conclusions or recommendations expressed in this material are those of the author(s) and do not necessarily reflect the views of the National Science Foundation. LB and GJS would also like to acknowledge NSF DMREF award 1729487.

This work made use of the IMSERC Crystallography facility at Northwestern University, which has received support from the Soft and Hybrid Nanotechnology Experimental (SHyNE) Resource (NSF ECCS-2025633), and Northwestern University.

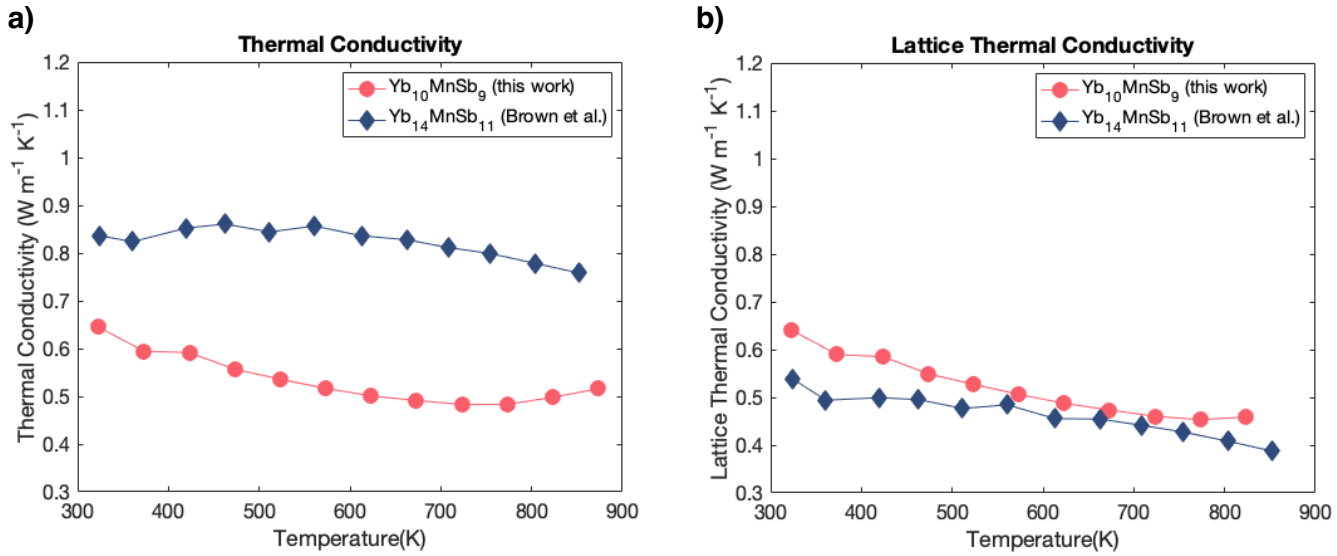

Fig. 3 Thermal properties of $Yb_{10}MnSb_9$ as compared with reported data for $Yb_{14}MnSb_{11}$ [24]. (a) The total thermal conductivity as a function of temperature. Here it is shown that $Yb_{10}MnSb_9$ has an ultra-low thermal conductivity, even lower than that of leading thermoelectric material $Yb_{14}MnSb_{11}$. (b) The lattice thermal conductivity as a function of temperature, calculated by subtracting the electronic thermal conductivity from the total thermal conductivity. While $Yb_{10}MnSb_9$, has a lower total thermal conductivity than $Yb_{14}MnSb_{11}$, it has a slightly higher lattice thermal conductivity. This can be attributed to the much higher electrical resisitivity in the $Yb_{10}MnSb_9$ sample.

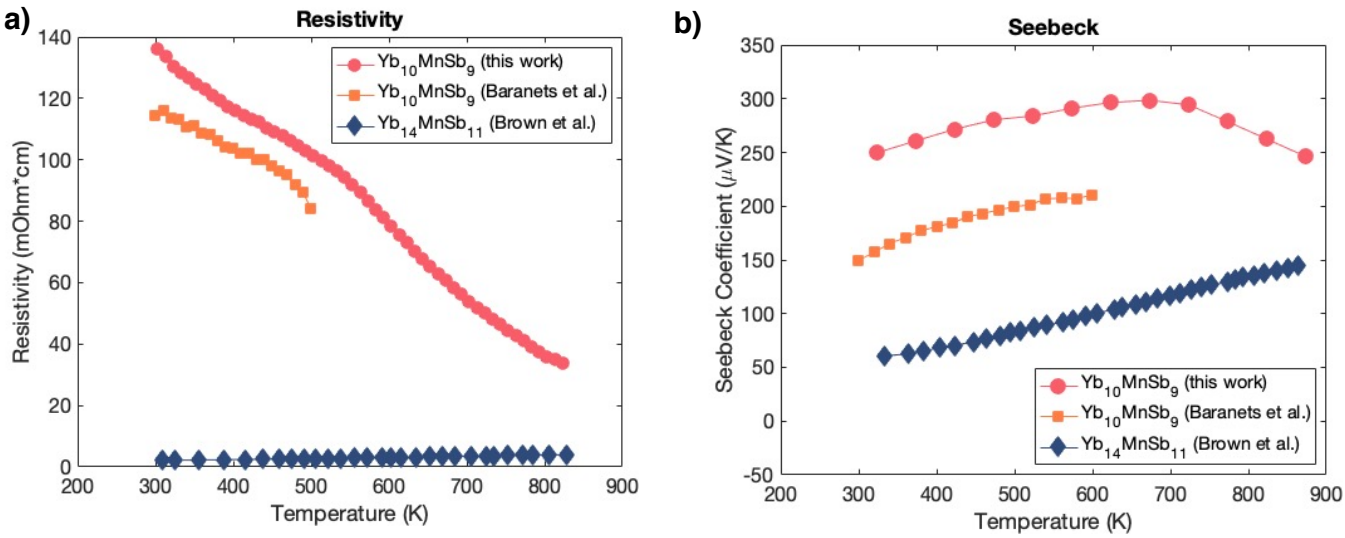

Fig. 4 Electronic properties of $Yb_{10}MnSb_9$ as compared with previously reported values for this compound [28] as well as $Yb_{14}MnSb_{11}$ [24]. For both the sample reported here as well as previously reported 10-1-9 data, the sample is highly resistive, much more so than 14-1-11 and has a high Seebeck coefficient. It can also be noted that the 10-1-9 sample reported here has both a larger electrical resistivity and Seebeck coefficient, indicative of different charge carrier concentrations.

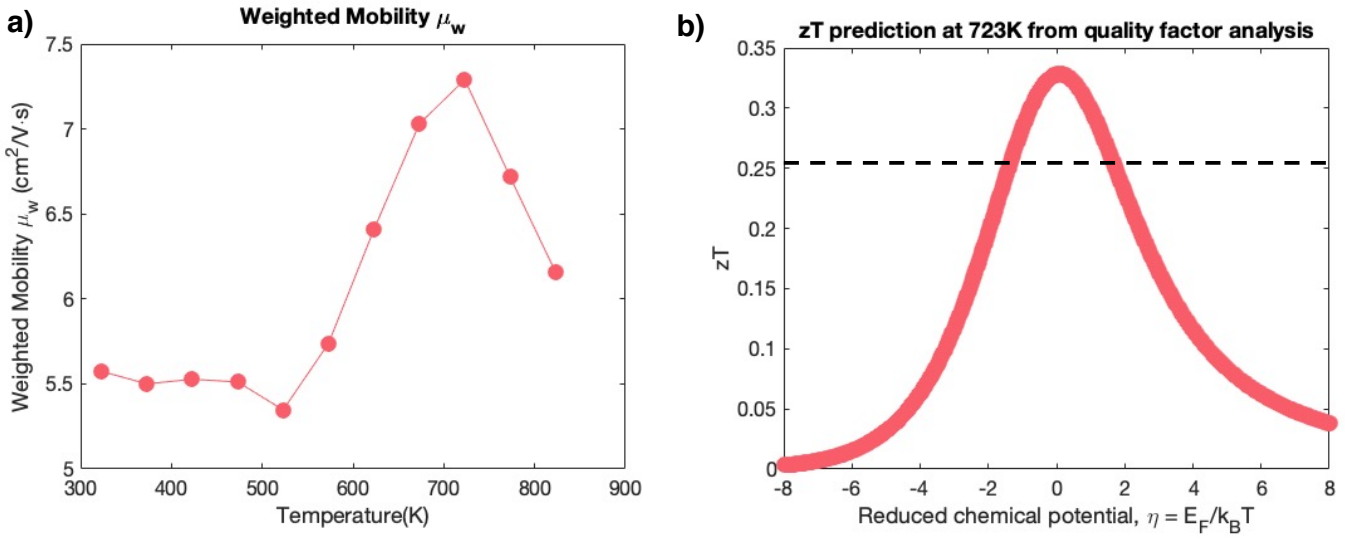

Fig. 5 a) Plot of weighted mobility as calculated from the Seebeck coefficient and electrical conductivity[58] as a function of temperature. Here we can see an increase in weighted mobility until the onset of bipolar conduction at high temperatures. b) zT curve as a function of the reduced chemical potential, η calculated using the thermoelectric quality factor B at 725K (B=0.0962). From this we estimate that given appropriate doping, $Yb_{10}MnSb_9$ should reach a zT value of about 0.33 at a temperature of 723K. The black dashed line indicates the experimental zT at 725K, indicating that further improvements can be made via doping.

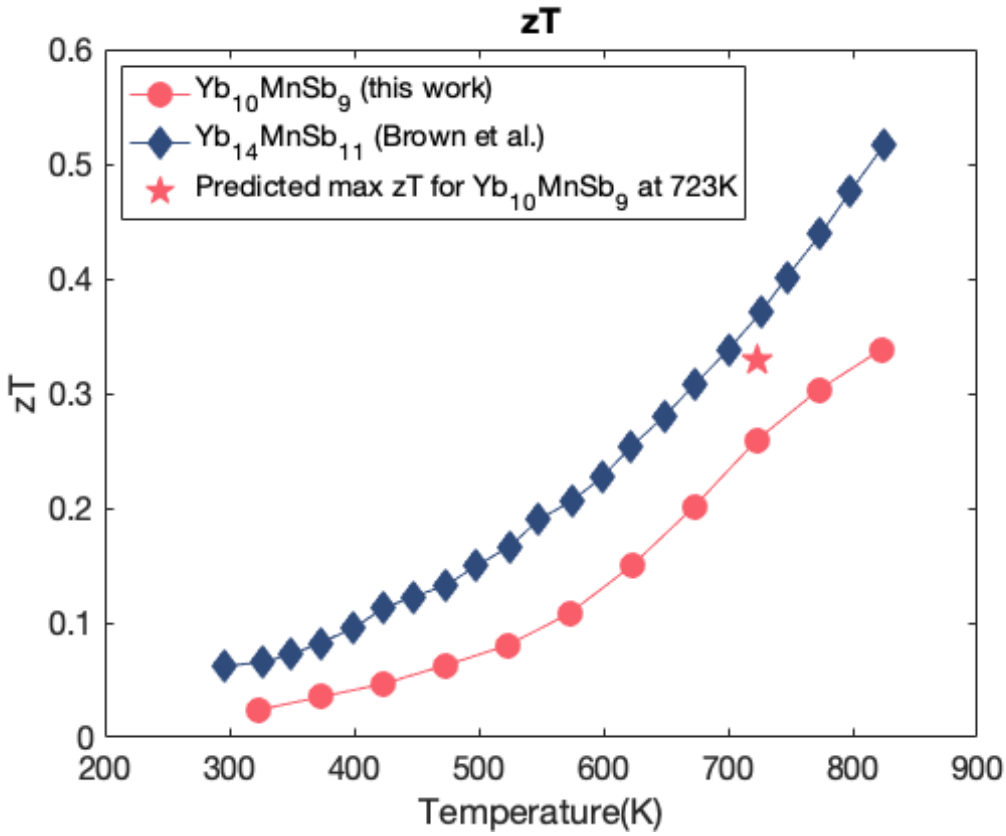

Fig. 6 The dimensionless thermoelectric figure of merit, zT vs. temperature for this work as compared with reported data for $Yb_{14}MnSb_{11}$[24]. The star indicates the expected zT of $Yb_{10}MnSb_9$ given optimal doping at 725K. This maximum zT at 725K was determined using the quality factor analysis. By calculating the quality factor at a given temperature using measurements of thermal conductivity, κ, electrical conductivity, σ, and the Seebeck coefficient, S, the relationship between the value of zT and the reduced chemical potential, η can be plotted as shown in Figure 5b, giving us the maximum zT for this material given optimized doping at 725K.

Notes and references

1 T. C. Holgate, R. Bennett, T. Hammel, T. Caillat, S. Keyser and B. Sievers, *Journal of Electronic Materials*, 2015, **44**, 1814–1821.

2 G. J. Snyder and E. S. Toberer, *Nature Materials*, 2008, **7**, 105–114.

3 E. Zintl and W. Dullenkopf, *Z. Phys. Chem., Abt. B*, 1932, **16**, 183–194.

4 E. Zintl and G. Brauer, *Zeitschrift für Physikalische Chemie*, 1933, **20**, 245–271.

5 E. Zintl, *Angewandte Chemie*, 1939, **52**, 1–6.

6 J. H. Grebenkemper, Y. Hu, D. Barrett, P. Gogna, C. K. Huang, S. K. Bux and S. M. Kauzlarich, *Chemistry of Materials*, 2015, **27**, 5791–5798.

7 A. He, E. L. Wille, L. M. Moreau, S. M. Thomas, J. M. Lawrence, E. D. Bauer, C. H. Booth and S. M. Kauzlarich, *Physical Review Materials*, 2020, **4**, 114407.

8 E. S. Toberer, C. A. Cox, S. R. Brown, T. Ikeda, A. F. May, S. M. Kauzlarich and G. Jeffrey Snyder, *Advanced Functional Materials*, 2008, **18**, 2795–2800.

9 Y. Hu, G. Cerretti, E. L. Kunz Wille, S. K. Bux and S. M. Kauzlarich, *Journal of Solid State Chemistry*, 2019, **271**, 88–102.

10 A. Zevalkink, E. S. Toberer, W. G. Zeier, E. Flage-Larsen and G. J. Snyder, *Energy and Environmental Science*, 2011, **4**, 510–518.

11 A. F. May, E. S. Toberer, A. Saramat and G. J. Snyder, *Physical Review B - Condensed Matter and Materials Physics*, 2009, **80**, 1–12.

12 A. Bhardwaj, N. S. Chauhan, S. Goel, V. Singh, J. J. Pulikkotil, T. D. Senguttuvan and D. K. Misra, *Physical Chemistry Chemical Physics*, 2016, **18**, 6191–6200.

13 S. J. Andersen, R. Holmestad and C. D. Marioara, Proceedings of JCNCS 2010, 2010, pp. 1–4.

14 M. Wood, M. Y. Toriyama, S. Dugar, J. Male, S. Anand, V. Stevanović and G. J. Snyder, *Advanced Energy Materials*, 2021, **11**, DOI:10.1002/aenm.202100181.

15 G. J. Snyder, M. Christensen, E. Nishibori, T. Caillat and B. B. Iversen, *Nature Materials*, 2004, **3**, 458–463.

16 S. M. Kauzlarich, A. Zevalkink, E. Toberer and G. J. Snyder, *RSC Energy and Environment Series*, 2017, **2017-January**, 1–26.

17 H. Luo, J. W. Krizan, L. Muechler, N. Haldolaarachchige, T. Klimczuk, W. Xie, M. K. Fuccillo, C. Felser and R. J. Cava, *Nature Communications*, 2015, **6**, DOI: 10.1038/ncomms7489.

18 *Chemistry, Structure, and Bonding of Zintl Phases and Ions (Chemistry of Metal Clusters)*, ed. S. M. Kauzlarich, Vch Pub, Hardcover edn, 1996.

19 W. G. Zeier, J. Schmitt, G. Hautier, U. Aydemir, Z. M. Gibbs, C. Felser and G. J. Snyder, *Nature Reviews Materials*, 2016, **1**, DOI:10.1038/natrevmats.2016.32.

20 E. S. Toberer, A. F. May and G. J. Snyder, *Chemistry of Materials*, 2010, **22**, 624–634.

21 J. Shuai, J. Mao, S. Song, Q. Zhang, G. Chen and Z. Ren, *Materials Today Physics*, 2017, **1**, 74–95.

22 S. M. Kauzlarich, S. R. Brown and G. Jeffrey Snyder, *Journal of the Chemical Society. Dalton Transactions*, 2007, 2099–2107.

23 J. Y. Chan, M. M. Olmstead, S. M. Kauzlarich and D. J. Webb, *Chemistry of Materials*, 1998, **36**, 3583–3588.

24 S. R. Brown, S. M. Kauzlarich, F. Gascoin and G. Jeffrey Snyder, *Chemistry of Materials*, 2006, **18**, 1873–1877.

25 G. Cerretti, O. Villalpando, J. P. Fleurial and S. K. Bux, *Journal of Applied Physics*, 2019, **126**, DOI:10.1063/1.5118227.

26 C. J. Perez, M. Wood, F. Ricci, G. Yu, T. Vo, S. K. Bux, G. Hautier, G.-m. Rignanese, G. J. Snyder and S. M. Kauzlarich, *Science Advances*, 2021, **7**, DOI: 10.1126/sciadv.abe9439.

27 A. He, S. K. Bux, Y. Hu, D. Uhl, L. Li, D. Donadio and S. M. Kauzlarich, *Chemistry of Materials*, 2019, **31**, 8076–8086.

28 S. Baranets, A. Ovchinnikov and S. Bobev, *Inorganic Chemistry*, 2021, **60**, 6702–6711.

29 A. Ovchinnikov, S. Chanakian, A. Zevalkink and S. Bobev, *Chemistry of Materials*, 2021, **33**, 3172–3186.

30 A. K. Ganguli, S. Gupta and J. D. Corbett, *Inorganic Chemistry*, 2006, **45**, 196–200.

31 S. Bobev, V. Fritsch, J. D. Thompson, J. L. Sarrao, B. Eck, R. Dronskowski and S. M. Kauzlarich, *Journal of Solid State Chemistry*, 2005, **178**, 1071–1079.

32 T. Yi, C. A. Cox, E. S. Toberer, G. J. Snyder and S. M. Kauzlarich, *Chemistry of Materials*, 2010, **22**, 935–941.

33 S.-q. Xia, J. Hullmann, S. Bobev, A. Ozbay, E. R. Nowak and V. Fritsch, *Journal of Solid State Chemistry*, 2007, **180**, 2088–2094.

34 S. Kastbjerg, C. A. Uvarov, S. M. Kauzlarich, Y. S. Chen, E. Nishibori, M. A. Spackman and B. B. Iversen, *Dalton Transactions*, 2012, **41**, 10347–10353.

35 S. Q. Xia and S. Bobev, *Chemistry of Materials*, 2010, **22**, 840–850.

36 Y. Y. Wang, S. Xu, L. L. Sun and T. L. Xia, *Physical Review Materials*, 2018, **2**, 1–6.

37 R. Rühl and W. Jeitschko, *Materials Research Bulletin*, 1979, **14**, 513–517.

38 A. Jain, S. P. Ong, G. Hautier, W. Chen, W. D. Richards, S. Dacek, S. Cholia, D. Gunter, D. Skinner, G. Ceder and K. a. Persson, *APL Materials*, 2013, **1**, 011002.

39 J. E. Saal, S. Kirklin, M. Aykol, B. Meredig and C. Wolverton, *Jom*, 2013, **65**, 1501–1509.

40 S. Kirklin, J. E. Saal, B. Meredig, A. Thompson, J. W. Doak, M. Aykol, S. Rühl and C. Wolverton, *npj Computational Materials*, 2015, **1**, DOI:10.1038/npjcompumats.2015.10.

41 K. P. Devlin, J. H. Grebenkemper, K. Lee, G. Cerretti, S. K. Bux and S. M. Kauzlarich, *Chemistry of Materials*, 2020, **32**, 9268–9276.

42 A. P. Justl, G. Cerretti, S. K. Bux and S. M. Kauzlarich, *Chemistry of Materials*, 2022, **34**, 1342–1355.

43 A. D. LaLonde, T. Ikeda and G. J. Snyder, *Review of Scientific Instruments*, 2011, **82**, 1–4.

44 K. A. Borup, E. S. Toberer, L. D. Zoltan, G. Nakatsukasa,

M. Errico, J. P. Fleurial, B. B. Iversen and G. J. Snyder, *Review of Scientific Instruments*, 2012, **83**, DOI:10.1063/1.4770124.

45 S. Iwanaga, E. S. Toberer, A. Lalonde and G. J. Snyder, *Review of Scientific Instruments*, 2011, **82**, DOI:10.1063/1.3601358.

46 H. M. Rietveld, *Journal of Applied Crystallography*, 1969, **2**, 65–71.

47 B. H. Toby and R. B. Von Dreele, *Journal of Applied Crystallography*, 2013, **46**, 544–549.

48 R. Hanus, R. Gurunathan, L. Lindsay, M. T. Agne, J. Shi, S. Graham and G. Jeffrey Snyder, *Applied Physics Reviews*, 2021, **8**, DOI:10.1063/5.0055593.

49 L. Borgsmiller, D. Zavanelli and G. J. Snyder, *PRX Energy*, submitted 2022.

50 S. Ohno, U. Aydemir, M. Amsler, J. H. Pöhls, S. Chanakian, A. Zevalkink, M. A. White, S. K. Bux, C. Wolverton and G. J. Snyder, *Advanced Functional Materials*, 2017, **27**, year.

51 S. Ohno, K. Imasato, S. Anand, H. Tamaki, S. D. Kang, P. Gorai, H. K. Sato, E. S. Toberer, T. Kanno and G. J. Snyder, *Joule*, 2018, **2**, 141–154.

52 Y. Tang, Y. Qiu, L. Xi, X. Shi, W. Zhang, L. Chen, S. M. Tseng, S. W. Chen and G. J. Snyder, *Energy and Environmental Science*, 2014, **7**, 812–819.

53 Y. Tang, S. wen Chen and G. J. Snyder, *Journal of Materiomics*, 2015, **1**, 75–84.

54 Y. Tang, X. Li, L. H. Martin, E. Cuervo Reyes, T. Ivas, C. Leinenbach, S. Anand, M. Peters, G. J. Snyder and C. Battaglia, *Energy and Environmental Science*, 2018, **11**, 311–320.

55 Y. Tang, R. Hanus, S. W. Chen and G. J. Snyder, *Nature Communications*, 2015, **6**, 1–7.

56 H. J. Goldsmid and J. W. Sharp, *Journal of Electronic Materials*, 1999, **28**, 869–872.

57 S. K. Bux, A. Zevalkink, O. Janka, D. Uhl, S. Kauzlarich, J. G. Snyder and J. P. Fleurial, *Journal of Materials Chemistry A*, 2014, **2**, 215–220.

58 G. J. Snyder, A. H. Snyder, M. Wood, R. Gurunathan, B. H. Snyder and C. Niu, *Advanced Materials*, 2020, **32**, 1–5.

59 Y. Pei, H. Wang and G. J. Snyder, *Advanced Materials*, 2012, **24**, 6125–6135.

60 S. D. Kang and G. Jeffrey Snyder, *Advances in Thermoelectricity: Foundational Issues, Materials and Nanotechnology*, 2021, 27–36.

61 E. S. Toberer, C. A. Cox, S. R. Brown, T. Ikeda, A. F. May, S. M. Kauzlarich and G. Jeffrey Snyder, *Advanced Functional Materials*, 2008, **18**, 2795–2800.

62 T. Yi, M. N. Abdusalyamova, F. Makhmudov and S. M. Kauzlarich, *Journal of Materials Chemistry*, 2012, **22**, 14378–14384.

63 S. R. Brown, E. S. Toberer, T. Ikeda, C. A. Cox, F. Gascoin, S. M. Kauzlarich and G. J. Snyder, *Chemistry of Materials*, 2008, **20**, 3412–3419.

64 S. Ohno, A. Zevalkink, Y. Takagiwa, S. K. Bux and G. J. Snyder, *Journal of Materials Chemistry A*, 2014, **2**, 7478–7483.

65 K. Imasato, C. Fu, Y. Pan, M. Wood, J. J. Kuo, C. Felser and G. J. Snyder, *Advanced Materials*, 2020, **32**, DOI:10.1002/adma.201908218.

66 M. Wood, J. J. Kuo, K. Imasato and G. J. Snyder, *Advanced Materials*, 2019, **31**, DOI:10.1002/adma.201902337.

67 Y. Lin, M. Wood, K. Imasato, J. J. Kuo, D. Lam, A. N. Mortazavi, T. J. Slade, S. A. Hodge, K. Xi, M. G. Kanatzidis, D. R. Clarke, M. C. Hersam and G. J. Snyder, *Energy and Environmental Science*, 2020, **13**, 4114–4121.

68 S. Li, Z. Huang, R. Wang, C. Wang, W. Zhao, N. Yang, F. Liu, J. Luo, Y. Xiao and F. Pan, *Journal of Materials Chemistry A*, 2021, **9**, 11442–11449.

69 P. A. Zong, R. Hanus, M. Dylla, Y. Tang, J. Liao, Q. Zhang, G. J. Snyder and L. Chen, *Energy and Environmental Science*, 2017, **10**, 183–191.

70 N. A. Pieczulewski, M. Wood, M. Y. Toriyama, J. P. Male, K. J. Griffith and G. J. Snyder, *MRS Communications*, 2021, **11**, 226–232.